

# Interface roughness, carrier localization and wave function overlap in *c*-plane InGaN/GaN quantum wells: Interplay of well width, alloy microstructure, structural inhomogeneities and Coulomb effects

Daniel S. P. Tanner,<sup>1</sup> Joshua M. McMahon,<sup>1</sup> and Stefan Schulz<sup>1</sup>

<sup>1</sup>*Photonics Theory Group, Tyndall National Institute,  
University College Cork, Cork, T12 R5CP, Ireland*

(Dated: February 2, 2022)

In this work we present a detailed analysis of the interplay of Coulomb effects and different mechanisms that can lead to carrier localization effects in *c*-plane InGaN/GaN quantum wells. As mechanisms for carrier localization we consider here effects introduced by random alloy fluctuations as well as structural inhomogeneities such as well width fluctuations. Special attention is paid to the impact of the well width on the results. All calculations have been carried out in the framework of atomistic tight-binding theory. Our theoretical investigations show that independent of the here studied well widths, carrier localization effects due to built-in fields, well width fluctuations and random alloy fluctuations dominate over Coulomb effects in terms of charge density redistributions. However, the situation is less clear cut when the well width fluctuations are absent. For large well width (approx.  $> 2.5$  nm) charge density redistributions are possible but the electronic and optical properties are basically dominated by the spatial out-of plane carrier separation originating from the electrostatic built-in field. The situation changes for lower well width ( $< 2.5$  nm) where the Coulomb effect can lead to significant charge density redistributions and thus might compensate a large fraction of the spatial in-plane wave function separation observed in a single-particle picture. Given that this in-plane separation has been regarded as one of the main drivers behind the green gap problem, our calculations indicate that radiative recombination rates might significantly benefit from a reduced quantum well barrier interface roughness.

## I. INTRODUCTION

Over the last several years, the theoretical and experimental analysis of carrier localization effects in InGaN/GaN quantum wells (QWs) has been of strong interest,<sup>1–4</sup> and has recently gathered enormous pace.<sup>5–16</sup> This stems from the fact that a detailed understanding of this question is important not only from a fundamental physics point of view, but also for device applications.<sup>4</sup> Indeed, carrier localization is widely accepted to be the reason that modern light emitting devices based on InGaN/GaN QWs, with their high density of defects, are able to function at all.<sup>4</sup> Furthermore, carrier localization is essential to explain the optical properties of this material system in detail. For example, the photoluminescence (PL) spectra of these InGaN/GaN QWs exhibit large line widths,<sup>3,17</sup> an “S-shaped” temperature dependence of the PL peak energy,<sup>1,6</sup> a mobility edge,<sup>18</sup> and a time-decay behavior where the explanation depends crucially on localization effects.<sup>2,9</sup>

The cause, nature, and consequence of this localization has generated significant debate over the years. Initially localization in InGaN was attributed to observed In rich clusters<sup>19</sup> purportedly forming due to the theoretically determined immiscibility of the alloy.<sup>20</sup> However, careful transmission electron microscopy (TEM)<sup>21</sup> and detailed atomic force microscopy (AFM) measurements<sup>22</sup> found the observed clusters to be artifacts of the measurement technique. Additionally, when studies accounted for the strain in InGaN QWs, originating from an underlying substrate, it was demonstrated that the miscibility limit is higher than predicted from a calculation

where this aspect is neglected.<sup>23</sup> Since these developments, localization in *c*-plane InGaN QWs has been primarily attributed to random alloy fluctuations<sup>5,8,10–12,15</sup> along with features introduced by the interplay of built-in field and well width fluctuations (WWFs),<sup>5,8,10</sup> which have been observed in several experimental studies.<sup>3,24</sup> The relationship between these mechanisms of localization and the manner in which the electrons and holes are respectively localized, and the consequences of this localization, stand as the next challenge to the full understanding and optimization of InGaN QW-based light emitting devices. This originates from the fact that recently two of the major roadblocks for future energy efficient light emission from InGaN-based LEDs, namely the “green gap” and the “droop” phenomenon, have been tightly linked to carrier localization features and interfacial roughness.<sup>7,11–13,15,25</sup>

For instance, interfacial roughness between an InGaN QW and the GaN barrier has been considered a key factor for increasing Auger recombination rates, as shown by Tan *et al.*<sup>25</sup> Several studies have reported that Auger recombination is the main driver behind the efficiency droop problem, which describes the reduction in the efficiency of InGaN-based LEDs with increasing current density.<sup>26–29</sup> In a separate theoretical study, which neglected WWFs, Jones *et al.*<sup>12</sup> demonstrated that compared to virtual crystal approximation (VCA) calculations, calculations including alloy induced carrier localization features reveal increased Auger recombination rates in InGaN QW systems. Both the work of Tan *et al.*<sup>25</sup> and Jones *et al.*<sup>12</sup> build on the same underlying concept that *k*-selection rules are broken due to al-

loy/interfacial roughness induced localization. This highlights that understanding the effect of WWFs and alloy fluctuations on the electronic and optical properties of *c*-plane InGaN QWs in detail is not only of interest from a fundamental perspective but also from a device application point of view.

The understanding of these features is also relevant to the green gap problem. This describes the drop in efficiency of InGaN/GaN emitters in the green to yellow spectral range when compared to blue emitters. Auf der Maur *et al.*<sup>11</sup> analyzed the contribution of random alloy effects to the green gap phenomenon. The authors<sup>11</sup> draw the conclusion that not only does the built-in field serve to decrease the radiative recombination rate, but so too does the spatially in-plane separation of the carriers due to localization features induced by the random alloy. Using as a reference a calculation based on a VCA, the authors concluded that this in-plane separation contributed as much as 30% to the reduction of the radiative recombination rate in green-emitting QWs.<sup>11</sup> A similar conclusion was reached by Karpov using an empirical model.<sup>13</sup>

However, it should be noted that a recent investigation by Jones *et al.*<sup>12</sup> contradicted this result. Using a modified continuum-based approach, accounting for random alloy fluctuations and connected carrier localization effects, Jones *et al.*<sup>12</sup> showed that random alloy fluctuations are beneficial for the radiative recombination rate. This is based, again, on the argument that with random alloy fluctuations, *k*-selection rules for transitions between different electron and hole states are no longer valid. Thus, even though the dipole matrix elements are reduced by carrier localization effects and the connected spatial separation of electron and hole wave functions, a significantly increased number of transitions are allowed when compared to a VCA treatment. So, taking all this into account, the impact of carrier localization effects on the optical properties and in particular on the question of the green gap problem, which is crucial for device applications, is still surrounded by controversy as is the underlying physics of these systems in general.

In addition to their disagreement on the impact of alloy fluctuations on the radiative recombination in InGaN devices, these previous theoretical studies have also neglected two important aspects of typical InGaN/GaN QWs. First, the above discussed studies do not account for structural inhomogeneities such as WWFs. These structural features, in tandem with the strong built-in fields in *c*-plane InGaN QWs, have been found to localize electron wave functions,<sup>8,30</sup> and can therefore strongly contribute to the in-plane carrier separation. If the in-plane carrier localization features are central to the green gap problem, then WWFs, by inducing further in-plane separation, should worsen the reduction in efficiency. Therefore, a detailed understanding of the impact of the interface roughness is required for the optimization of devices to ameliorate the green gap problem.

Second, an additional component when studying the

importance of in-plane carrier localization for optical properties are Coulomb effects. These effects have been widely neglected in the theoretical studies that account for carrier localization features in InGaN/GaN QWs. This leads to the question of whether or not Coulomb effects can reduce the spatial in-plane carrier separation. Given that the electrostatic built-in field strongly spatially separates electron and hole wave functions along the growth direction, the importance of Coulomb effects should increase with decreasing well width. In this respect, the question remains if carrier localization due the combination of WWFs, built-in field and random alloy fluctuations dominates over the attractive Coulomb interaction between electron and hole. Most of the above discussed theoretical studies have been either based on single-particle results,<sup>5,10–12,14</sup> in the absence of WWFs, or for a fixed well width.<sup>11,12,14</sup> In studies including Coulomb effects and carrier localization, a fixed well width and a high In content of 25% has been targeted so far.<sup>8</sup>

Finally, if Coulomb effects do indeed gain significance when structural well parameters change, the recombination dynamics of the system could change drastically, which again could be of benefit for InGaN-based devices with improved radiative recombination rates. An important early connection between carrier localization mechanisms and the distinctive optical properties of InGaN/GaN QWs was demonstrated by Morel *et al.*<sup>2</sup> Here, Morel and co-workers<sup>2</sup> applied a model of independently localized electrons and holes (pseudo two-dimensional donor-acceptor pair system) to describe the *non-exponential* decay curves in time-resolved PL measurements of *c*-plane InGaN/GaN QW systems. In contrast, other studies on *c*-plane InGaN/GaN QWs reported time-resolved PL measurements in which the PL decay curves exhibit a *single exponential* behavior.<sup>31</sup> Such behavior can be attributed to exciton localization effects, where, for instance, the hole is strongly localized and the electron localizes about the hole.<sup>9</sup> Therefore, as already indicated above, the recombination dynamics (non-exponential vs. single exponential) can be affected and ideally may be tuned by a variety of different factors such as well width,<sup>31</sup> In content,<sup>32,33</sup> or as we will show, the interface roughness. Taking all of the above into consideration, understanding the interplay of Coulomb effects, interfacial roughness and carrier localization mechanisms is obviously interesting from a fundamental physics view point but is also key for device design.

In this work we undertake the analysis of the interplay of carrier localization mechanisms, introduced by (random) alloy fluctuations, WWFs and Coulomb effects and we comment here on the connected impact on the optical (radiative) properties of InGaN/GaN QWs. Special attention is paid to the influence of the well width on the results. The calculations have been carried in an atomistic tight-binding (TB) framework, allowing us to gain insight into these questions on a microscopic level.

Here, we have studied *c*-plane InGaN/GaN QWs with a well width varying between 1.6 nm and 3.4 nm. For this analysis we have used an “intermediate” In content of 15%. By studying identical QWs with and without WWFs, we demonstrate the significant impact that WWFs have on the localization of electron states, even for smaller well width (1.6 nm). Independent of well width, this picture is mainly unchanged when Coulomb effects are included and carrier localization features remain dominated by WWFs (electron) and random alloy fluctuations (hole). For higher In contents, usually realized for emitters operating in the green spectral range, this effect will be even more pronounced.<sup>10</sup>

The situation in the absence of WWFs is less clear cut. Here, the single-particle electron wave function exhibits a more delocalized nature with perturbations introduced by the local alloy structure. When including Coulomb effects, even for the larger well width, our calculations exhibit a redistribution of the electron charge density. When turning to systems with a lower well width, Coulomb effects can significantly affect the spatial in-plane carrier separation. Here, we observe that in the absence of the WWFs the electron wave function is much more likely to localize about the hole, thus resulting in exciton localization-like features. Overall, when looking at optical spectra, the benefits of this charge density redistribution are found to increase with decreasing width. This indicates that the out-of plane separation of the carriers dominates the wave function overlap at larger widths.

In general, our results show that reducing the interface roughness between GaN and InGaN in InGaN/GaN QWs, and thus ideally circumventing WWFs, should, due to Coulomb effects, reduce the in-plane spatial separation of electron and hole wave functions. Following the idea of Auf der Maur *et al.*<sup>11</sup>, the radiative recombination rate should benefit from this. Additionally, in the light of the arguments given by Jones *et al.*<sup>12</sup>, an increased wave function overlap along with the absence of *k*-selection rules should give a further improvement of the radiative recombination rate. Thus reducing the InGaN/GaN interface roughness could be a promising way forward to improve the radiative device characteristics of InGaN/GaN based light emitters across a wide range of emission wavelength.

The manuscript is organized as follows. In the following section we briefly review the theoretical framework used in our studies. Here, also the QW system and how WWFs and alloy microstructure are treated is discussed. Section III presents the results of our theoretical study. In a first step, Sec. III A, the impact of random alloy fluctuations and WWFs on the built-in potential are discussed. This is followed by the analysis of single-particle results in Sec. III B. The impact of Coulomb effects on optical properties is discussed in Sec. III C. In Sec. III D, we compare and relate our theoretical findings to experimental data, radiative recombination dynamics, and the connected importance for nitride-based optoelectronic de-

vices. Finally, in Sec. IV a summary and conclusions of our investigations are presented.

## II. THEORY AND QW SYSTEM

In this section we briefly review the theoretical framework and the QW model system applied in this work. We start in Sec. II A with the theoretical framework. In Sec. II B the supercell used in our calculations is introduced. Here, we discuss also aspects such as In atom distribution as well as structural inhomogeneities (well width fluctuations).

### A. Theoretical Framework

The full description of each of the ingredients of our theoretical framework has been presented in detail in our previous work.<sup>8</sup> Here, we summarize only the main points. The central component underlying our study of the electronic and optical properties of InGaN/GaN QWs on an atomistic level is a nearest neighbor *sp*<sup>3</sup> tight-binding (TB) model. This model takes input from a valence force field (VFF) model, implemented in LAMMPS.<sup>34</sup> The applied VFF approach is based on Martin’s model, introduced in Ref. 35, including therefore electrostatic effects. This model accurately captures deviations from the ideal wurtzite structure, such as the lattice constant *c/a* ratio. Given the atomistic nature of our VFF approach, the model takes into account that the number of In and Ga atoms in the nearest neighbor environment of a N atom varies. Using the VFF, the relaxed atomic positions in the alloyed and strained supercell can be determined, including therefore also alloy induced local variations in the bond length and corresponding strain fields. These relaxed atomic positions provide input for the strain corrections of the TB matrix elements.<sup>36</sup> Additionally, the relaxed atomic positions provide input for our recently developed local polarization theory.<sup>36</sup> In this approach, the total polarization vector field is divided into a macroscopic and local polarization contribution. The macroscopic part is related to clamped ion contributions (no relaxation of the internal degrees of freedom of the atoms), while the local part is evaluated per local tetrahedron accounting therefore for internal strain effects. Starting from the local polarization at the different lattice sites, the resulting built-in potential is calculated from a point dipole-model. This circumvents the problem of solving Poisson’s equation on a (non-uniform) wurtzite lattice, keeping in mind the relaxed atomic positions of the InGaN QW. The calculated built-in potential is included in the TB model as a site-diagonal correction, which is a widely used approximation.<sup>37–39</sup> It should be noted that we are here interested in the low carrier density regime (see below). Focussing on this regime helps to disentangle carrier localization effects arising from WWFs, alloy microstructure and Coulomb

effects, thus throwing light on the interplay of these different aspects. Therefore, a non-self-consistent TB calculation is sufficient for our purposes here. However, to account for potential charge carrier density redistributions, which could be important, for instance, for the green gap problem, as highlighted above in more detail, we include Coulomb effects in our calculations.

To include Coulomb effects, the TB single-particle states serve as input for configuration interaction calculations.<sup>40</sup> The calculations are restricted to excitonic effects, meaning that only one electron-hole pair is considered. We account here for the direct electron-hole interaction; exchange terms are neglected since the connected matrix elements are small compared to the direct part. To account for screening effects in the Coulomb interaction, which is intrinsically a complex problem,<sup>41,42</sup> we use here a simplified approach and assume an isotropic and material independent (static low frequency) dielectric constant. For GaN we employ the values from Nakamura and Chichibu ( $\epsilon_{\perp,0}^r = 7.87$ ,  $\epsilon_{\parallel,0}^r = 8.57$ ), resulting in a very good agreement between theory and experiment in terms of GaN exciton binding energies.<sup>43</sup> For InN we use the values from Ref. 44 ( $\epsilon_{\perp,0}^r = 13.1$ ,  $\epsilon_{\parallel,0}^r = 14.4$ ). Given that both for InN and GaN the values of the ordinary ( $\epsilon_{\perp,0}^r$ ) and extraordinary ( $\epsilon_{\parallel,0}^r$ ) component are very similar in magnitude, the isotropic approximation is reasonable. To obtain the InGaN dielectric constant, a linear interpolation between the InN and GaN values is applied. For the Coulomb calculations, this averaged dielectric constant is used for the entire supercell, justified by the observation that electron and hole wave functions are mainly localized inside the QW region (see below). Furthermore, as we will discuss below, we will study here only moderate In contents so that the dielectric constant contrast between well and barrier is small. Thus, the assumption of a position independent dielectric constant is a reasonable first approximation. Given that the screening of the Coulomb interaction should be distance dependent, our Coulomb matrix elements are split into a short-range and long-range part.<sup>45</sup> The short-range, on-site part is unscreened while for the long-range part the above approximation for the screening has been used. Similar approaches and approximations have been made in other systems.<sup>45–47</sup> In addition to Coulomb matrix elements, the TB wave functions have also been used to calculate dipole matrix elements.<sup>8,48</sup> In connection with many body wave functions and via Fermi's golden rule, the dipole matrix elements are used to calculate optical spectra. More details are given in Refs. 48 and 8.

## B. QW structure and simulation supercell

The TB calculations have been performed on wurtzite supercells with approximately 82,000 atoms. This corresponds to an overall system size of 10 nm x 9 nm x 10 nm with periodic boundary conditions. The QW width inside the supercell has been varied to investigate

the impact of this quantity on the electronic and optical properties of the system. The well width,  $L_w$ , is set to:  $L_w = 1.6$  nm,  $L_w = 2.11$  nm,  $L_w = 2.65$  nm and  $L_w = 3.43$  nm. As mentioned above, we are interested in investigating the influence of the well width on the electronic and optical properties of InGaN/GaN QWs; to do so, we keep the In content in the QW region fixed at 15%. Based on experimental studies,<sup>21,49</sup> we distribute In atoms randomly in the active region of the QW. It is important to note that in our atomistic framework, the In content at the QW barrier interface will locally vary. But, we do not account here for penetration of In atoms into the barrier. In the literature different In atom distribution profiles have been considered. Yang *et al.*<sup>7</sup> and McBride *et al.*<sup>50</sup> considered a Gaussian alloy distribution along the growth direction of *c*-plane InGaN QWs. However, several experimental studies have reported a sharp lower QW barrier interface (growth of InGaN on GaN), while the upper interface (GaN on InGaN) exhibited WWFs and some penetration of In into the barrier.<sup>49,51–55</sup> Watson-Parris<sup>30</sup> considered the effect of In incorporation in the barrier at the upper interface for a fixed well width (2.85 nm) and In content (25 %) on the basis of a modified continuum-based model, concluding that the inclusion of a diffuse upper interface has no noticeable effect on the results in terms of carrier localization. This indicates that for our present study the penetration of In atoms into the barrier is of secondary importance. This is further supported by the fact that the diffuseness of the In atoms in the QW plane is homogenous.<sup>5</sup> Thus, one could expect that the experimentally observed WWFs have a more significant impact on carrier localization effects when compared to the penetration of In atoms into the barrier. Finally, it should be noted that recent experimental studies have shown that by a careful choice of the growth procedure, the In incorporation in the barrier can significantly be reduced.<sup>55</sup> Therefore, the here made assumptions about the In distribution in the well and at the QW barrier interface should provide a good description of the experimentally observed systems.

In order to analyze the impact of the alloy microstructure on the results, the calculations have been repeated 20 times for each  $L_w$  value. To closely compare the results from the same configuration for different QW widths  $L_w$ , we proceed in the following way. We start with the lowest  $L_w$  values and generate the 20 different microscopic configurations. When studying the next largest system, for each configuration, we keep the random In atom configuration and just add new layers to the existing QW structure. For instance, for configuration (Config) 1 of a QW of width  $L_w = 2.11$  nm, the placement of In atoms in the first 12 atomic layers are identical to the placement of In atoms in the first 12 layers of the  $L_w = 1.6$  nm system for the same configuration. Likewise the first 20 atomic layers of Config *i* of the  $L_w = 2.85$  QW have identical In atom distributions to the 20 atomic layers in Config *i* forming the well



with  $L_w = 2.11$  nm. Thus, in terms of the In atom distribution, the lower QW-barrier interface is always the same for a given microscopic configuration, independent of the QW well width. In this way we are able to partially isolate the effects of well width and WWFs on the electronic and optical properties of the here considered  $\text{In}_{0.15}\text{Ga}_{0.75}\text{N}/\text{GaN}$  QWs from random alloy effects. Finally, all calculations have been performed in the presence and absence of WWFs. For the WWFs, following previous work,<sup>5,8,10,30</sup> we assume disk-like WWFs. The diameter of these fluctuations has been assumed to be 5 nm with a height of 2 monolayers, which is consistent with experimental observations.<sup>3,24</sup> In total 320 atomistic calculations have been performed to study the interplay of Coulomb effects, well width and carrier localization due to WWFs and random alloy fluctuations on the electronic and optical properties of  $\text{In}_{0.15}\text{Ga}_{0.85}\text{N}/\text{GaN}$  QWs.

### III. RESULTS

In this section we present the results of our atomistic analysis of the impact of well width and WWFs on the electronic and optical properties of  $c$ -plane  $\text{InGaN}/\text{GaN}$  QWs. Before turning to the electronic and optical properties, we start our discussion with a study of the electrostatic built-in potential and how alloy and WWFs affect this quantity. This investigation is presented in Sec. III A. Having discussed the built-in potential, we turn and present in Sec. III B the results of our TB analysis in the absence of Coulomb effects (single-particle data). In Sec. III C we discuss the impact of Coulomb (excitonic) effects on the results. Finally, we relate the here obtained theoretical results to experimental observations (Sec. III D).

#### A. Impact of random alloy and well width fluctuations on the built-in potential

To establish the impact of alloy and WWFs on the electrostatic built-in potential,  $V_p$ , Fig. 1 displays contour plots of  $V_p$  for different slices through the supercell of the same arbitrarily chosen microscopic configuration. The potential displayed is that of a QW of width  $L_w = 2.65$  nm. The contour plots are shown in the  $x - z$ -plane, where  $z$  is parallel to the wurtzite  $c$ -axis. The  $y$ -coordinate is varied, with increasing magnitude from left to right, resulting then in the different slices depicted in subsequent columns of Fig. 1. As a guide to eye, the (white) dashed lines indicate the QW interfaces. To ascertain the impact of interface roughness on the built-in potential: the upper row displays the result for a QW with a WWF ( $V_p^{\text{WWF}}$ ); the middle row gives the same QW configuration without a WWF ( $V_p^{\text{NoWWF}}$ ); and the last row shows the difference in the potential between a QW with and without a WWF,  $\Delta V_p = V_p^{\text{WWF}} - V_p^{\text{NoWWF}}$ . Several features of the built-in

potential are now of interest for our analysis.

First, in contrast to standard 1-D continuum-based approximations, which treat  $\text{InGaN}/\text{GaN}$  QW systems as an ideal system that can be described by average parameters, the built-in potential is strongly position dependent. This position dependence is manifested in Fig. 1 as isolines which are non-parallel. This is in contrast to the parallel isolines expected from a 1-D continuum-based, capacitor-like picture, where the potential is constant outside the well and has a well defined slope inside. Thus, the corresponding field is zero in the barrier and constant inside the QW. Second, the alloy fluctuations lead also to “pockets” in which the built-in potential significantly varies with respect to its environment. From this we infer already that random alloy fluctuations lead to significant changes in the built-in potential, both on a macroscopic as well as on a local, microscopic level. Third, turning now to the impact of the WWF, as expected, in the region of the WWF the built-in potential changes compared to the situation without the WWF. However, when looking at the last row of Fig. 1, we find also that the built-in potential underneath the WWF changes significantly compared to the situation in which no WWF has been considered. This originates from the fact that the disk-like WWF is a three dimensional object and that the strain field around this “QD-like” structure is changed. This has several consequences. Given that electron wave functions are localized at the upper interface of the QW and that the (alloy) microstructure of the upper layer with the inclusion or exclusion of a WWF changes, carrier localization features of these states are expected to be strongly affected. What might be less straightforward to predict *a priori* is that even though the alloy microstructure at the lower interface is not changed, the hole states which are localized at this interface, can be affected by the three-dimensional built-in potential effects discussed above. This aspect will be more pronounced in narrower wells. Therefore, introducing WWFs affects not only the effective volume of the QW, but also produces built-in potential modifications originating from the altered microscopic alloy configuration and strain relaxation of the system. Overall, the inclusion of the WWF also leads to a slight increase in the macroscopic built-in field compared to the system without WWFs. This is based on the observation of slightly negative (positive) built-in potential values below (above) the well, as it can be inferred from  $\Delta V_p$  (cf. last row of Fig. 1). Equipped with this knowledge, we turn now to analyze the electronic structure of  $\text{InGaN}/\text{GaN}$  QWs in the presence and absence of WWFs. Special attention is paid to the impact of the well width  $L_w$  on these properties. This will be the topic of the next two sections. We begin our analysis in the next section with an examination of single-particle results.

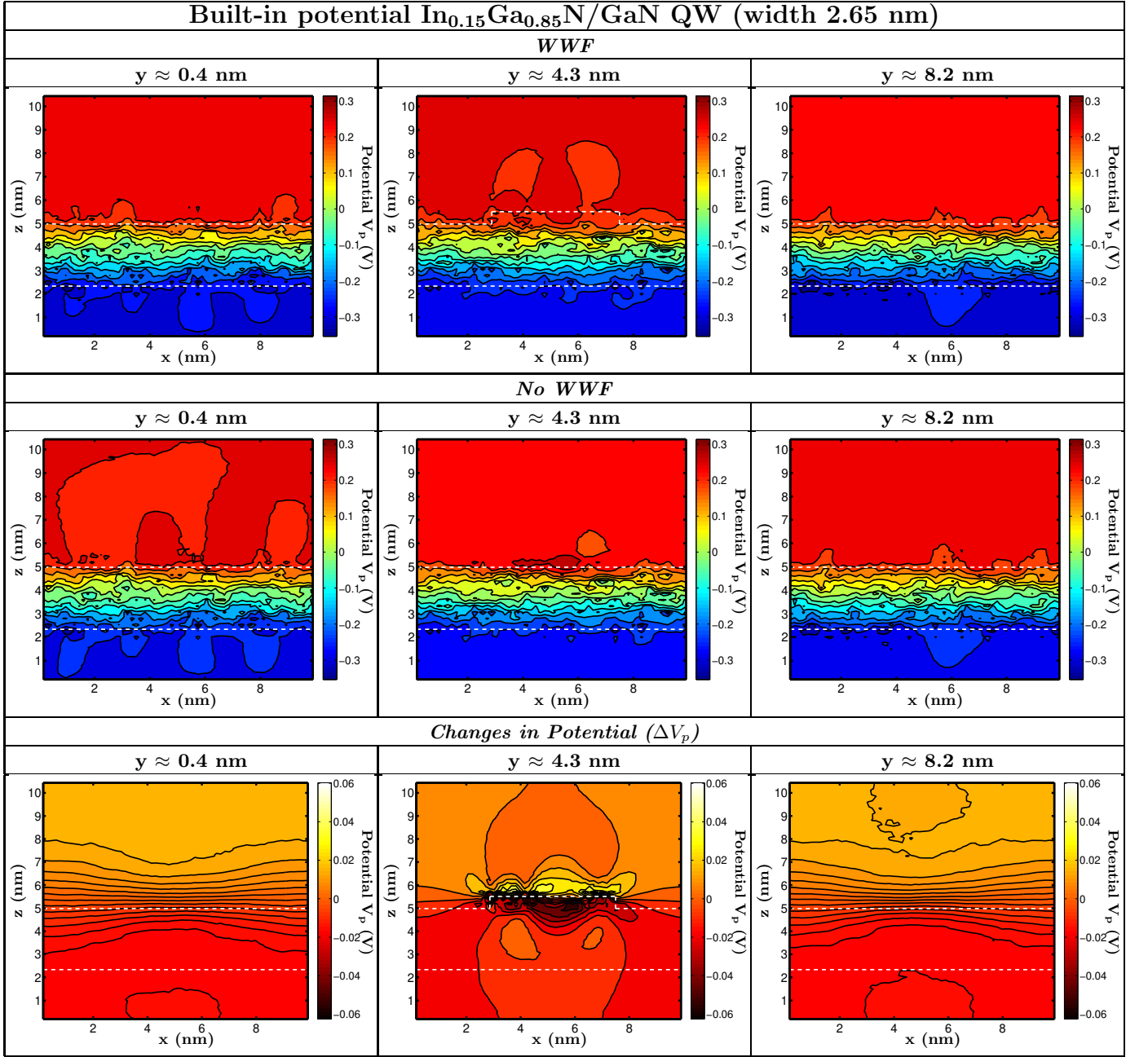


FIG. 1: (Color online) Contour plots of the electrostatic built-in potential  $V_p$  in the  $x$ - $z$ -plane of an  $\text{In}_{0.15}\text{Ga}_{0.85}\text{N}/\text{GaN}$  quantum well with well width  $L_w = 2.65$  nm. The  $z$ -axis is parallel to the wurtzite  $c$ -axis. The results are shown for different slices ( $y = 0.4$  nm;  $y = 4.3$  nm;  $y = 8.3$  nm) through the supercell of the same arbitrary microscopic configuration. The first row depicts the data for the quantum well where a disk-like well width fluctuation has been taken into account (*WWF*). The middle row displays the results for the same configuration and slices through the same planes as in the first row, however, this time in the absence of the well width fluctuation (*No WWF*). The last row depicts the difference in the potential  $\Delta V_p = V_p^{\text{WWF}} - V_p^{\text{No WWF}}$  between the situation with ( $V_p^{\text{WWF}}$ ) and without ( $V_p^{\text{No WWF}}$ ) the well width fluctuation calculated at the different  $y$ -coordinates.

### B. Impact of well width, random alloy and well width fluctuations on the electronic structure: Single-particle results

Figure 2 shows the single-particle (a) electron and (b) hole ground state (GS) energy as a function of the mi-

croscopic configuration number (Config #). The zero of energy for all these calculations is the unstrained GaN valence band edge. The data are shown for the different well width values ranging from  $L_w = 1.6$  nm to  $L_w = 3.43$  nm. The results where WWFs have been considered in the calculations are given by the filled symbols, while the

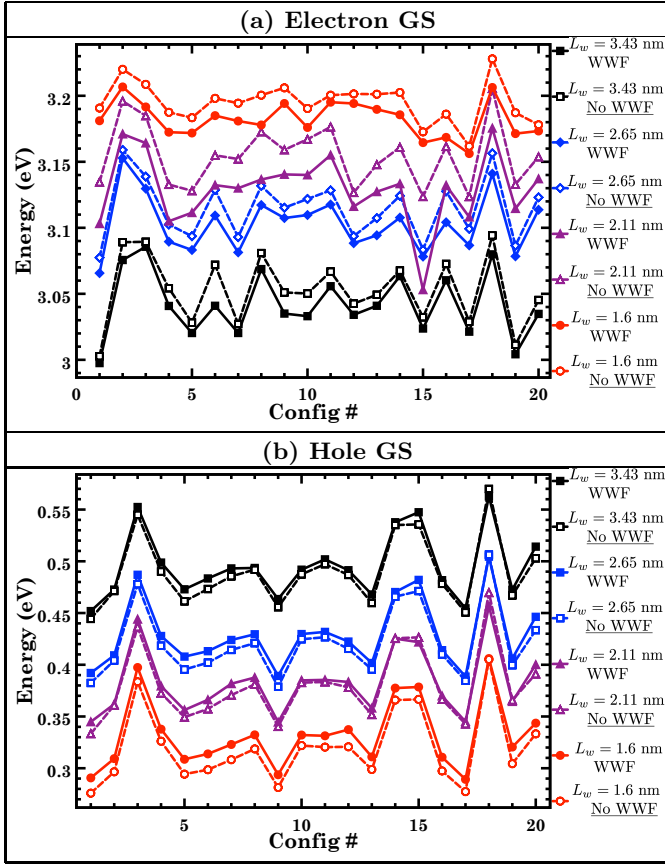


FIG. 2: Single-particle (a) electron and (b) hole ground state (GS) energy as a function of the microscopic configuration number (Config #). The data from calculations including well width fluctuations (WWF) are given by the filled symbols; the results when the well width fluctuation is absent are denoted by the open symbols (No WWF). The data are displayed for the different well widths  $L_w$ .

open symbols display the data in the absence of WWFs (No WWF). Overall, two important features should be taken into account before starting the detailed analysis of Fig. 2. First, due to the presence of the electrostatic built-in field along the growth direction (cf. Fig. 1), electron and hole wave functions are localized at opposite interfaces of the QW: electrons at the upper interface and holes at the lower interface.<sup>5</sup> Second, it is important to remember that WWFs are introduced at the upper QW interface. Thus, from a structural point of view, the lower interface for a given microscopic configuration is unchanged. From this perspective mainly electron GS energies should be affected by WWFs. Equipped with this information, several general features can be deduced from Fig. 2.

For both electrons and holes, the GS energies vary significantly with configuration number, though the holes show a much greater variance. This indicates that the alloy microstructure of the systems plays an important role. Additionally, for all widths,  $L_w$ , the inclusion of the

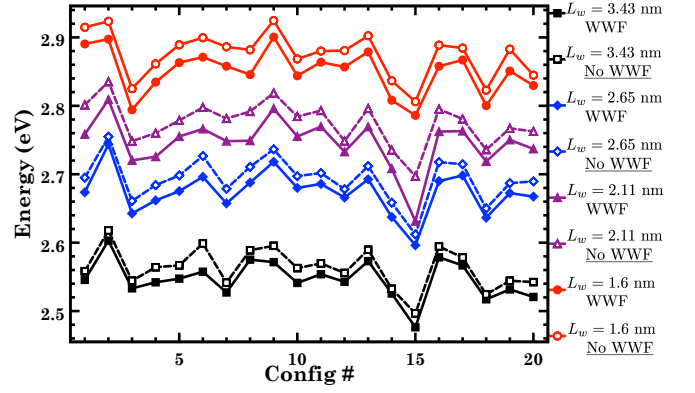


FIG. 3: Single particle transition energies as a function of the microscopic configuration number (Config #). The results are given for the different well widths  $L_w$ . Data in the absence of the well width fluctuation (No WWF) are denoted by the open symbols, while data in the presence of the well width fluctuation (WWF) are given by the filled symbols.

WWF shifts the electron GS energies to lower energies (cf. Fig. 2 (a)). Similarly for the hole GS energies (cf. Fig. 2 (b)), for all configurations but one (Config 18), the inclusion of the WWF leads to a shift to higher energies. We will come back to the particularities of Config. 18 further below.

For the electrons, Fig. 2 (a), we attribute the decrease in the GS energies to the slight increase in QW volume due to the WWFs and the overall slightly stronger built-in field in the system with WWFs when compared to structures without a WWF (cf. Sec. III A). Turning to the hole GS energy, even though the alloy microstructure at the lower interface is not changed by the addition of a WWF, the changes in the QW volume and the connected changes in built-in field due to the presence of the WWF (cf. Sec. III A) also affect the hole GS energy. However, when considering a given configuration, the changes in the hole ground state energies due to the presence of a WWF are in general smaller when compared to the changes in the electron GS energies.

The resulting changes in the electron and hole GS energies due to the presence of WWFs are summarized in Fig. 3. Here the GS *transition* energy for the different well widths is displayed as a function of the microscopic configuration number (Config #). For all well widths  $L_w$  we observe a red shift in the transition energy due to the presence of WWFs. This behavior reflects the trends in the electron and hole GS energies. This finding is also consistent with the simple picture that by including the WWF the well becomes effectively wider and that the built-in field slightly increases when compared to the QW without a WWF. Additionally, as expected from our analysis above, the GS transition energy varies significantly as a function of the configuration number. This behavior is consistent with the experimentally observed broad PL spectra in InGa<sub>N</sub>/Ga<sub>N</sub> QWs.<sup>3,56,57</sup>

Having established general features of how alloy fluctu-

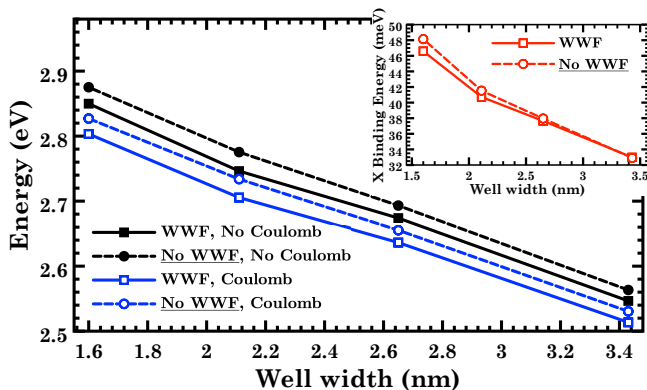


FIG. 4: Average transition energies with (WWF, squares) and without (No WWFs, circles) well width fluctuations as a function of the well width  $L_w$ . The data in the absence of Coulomb effects are given by the respective filled symbols while the open symbols denote the results when excitonic effects are taken into account. Inset: Exciton (X) binding energies in the presence (WWF, open squares) and absence (No WWF, open circles) of well width fluctuations as a function of the well width  $L_w$ .

ations and WWFs affect both electron and hole GS energies in a single-particle picture, we turn now and look at excitonic effects. Initially, we present an analysis of the (average) transition energy and also the exciton binding energy. In a second step we discuss how the Coulomb effect impacts carrier localization features.

### C. Impact of well width, random alloy and well width fluctuations on the electronic and optical properties: Excitonic effects

Figure 4 displays the *average* GS transition energies in the presence and absence of WWFs as a function of the well width  $L_w$ . Additionally, results with and without the inclusion of Coulomb effects in the calculations are given. The open (filled) symbols denote the results in the presence (absence) of excitonic effects. The squares (circles) show the data when WWFs are included (excludes) in the calculations. Thus, the filled symbols in Fig. 4 are obtained from averaging over the 20 different microscopic configurations presented in Fig. 3. The filled symbols in Fig. 4 confirm in a simple manner the aforementioned conclusion that the inclusion of WWFs result in a red shift of the transition energies. Figure 4 also illustrates clearly the increase in transition energy with decreasing  $L_w$ . Such a behavior is expected from a simple particle-in-box-like picture. Looking at the open symbols, we see that these expected trends also hold in the case where Coulomb effects are included.

Additionally, a comparison of the average transition energy with and without Coulomb effects allows for a first insight into the question of how the Coulomb interaction affects the optical properties of QWs with different

structural parameters. To facilitate this investigation, the inset in Fig. 4 depicts the exciton (X) binding energy in the presence (square) and absence (circle) WWFs, as a function of  $L_w$ . Here the exciton binding energy is defined as the difference in the average single particle GS transition energy and the calculated average excitonic transition energy. Three important features can be extracted from this inset: (i), the exciton binding energy increases with decreasing  $L_w$ ; (ii), in general the exciton binding energy decreases with inclusion of WWFs; and (iii), the impact of the WWF on the excitonic binding energy decreases with increasing  $L_w$  and turns out to be of secondary importance for large  $L_w$ . These results can be explained in terms of wave function overlaps: in a simplified picture one expects that the lower the spatial wave function overlap, the lower the excitonic binding energy. Thus, the decreasing vertical spatial separation of electron and hole wave functions with decreasing  $L_w$  accounts for the increase in excitonic binding. Secondly, if the electron wave functions are localized independently of  $L_w$  by the WWFs, then a further in-plane spatial separation, in addition to the out-of plane separation by the electrostatic built-in field, is expected. This in-plane separation can then lead to a further decrease in the excitonic binding energy when comparing the system with and without WWFs. Finally, the finding that removing the WWF has a reduced effect on the binding energies in wider than in narrower wells, is due to the fact that the strength of the Coulomb interaction is determined primarily by the vertical separation between the carriers. The fact that for larger values of  $L_w$  ( $L_w > 2.5$  nm) the average exciton binding energy is almost unaffected by the WWF, leads to the following interesting conclusion. Assuming that WWFs lead to an additional in-plane spatial separation between the carriers compared to a system without WWFs, the results of Fig. 4 indicate that the in-plane separation between the carriers is of secondary importance, at least in terms of the exciton binding energy. We will come back to this in Sec. III D, when we compare our theoretical data with experimental results and connect our theoretical findings also to radiative recombination characteristics. It should be noted that additional factors, such as the density and the statistical variations in size and shape of WWFs, could affect this result. These factors could further increase the in-plane spatial separation contribution.

So far we have only discussed *averaged* results and made assumptions about the nature of the carrier localization features. To corroborate these explanations of observed trends in the averaged properties and to investigate the interplay between well width, alloy microstructure, structural inhomogeneities and Coulomb effects, we present next an analysis of the electronic structure of the different QWs for different microscopic configurations. Figure 5 displays the exciton binding energies as a function of the configuration number (Config #). Here we have focused our attention on the extreme well width cases, thus  $L_w = 1.6$  nm (red circles) and  $L_w = 3.43$  nm



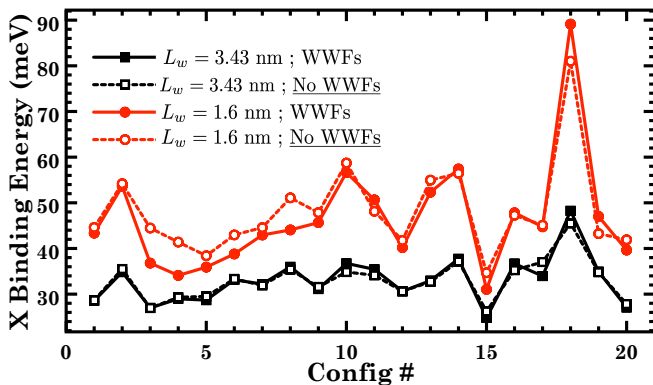


FIG. 5: Exciton (X) binding energy as a function of the microscopic configuration number (Config #). The results are shown for a well width of  $L_w = 1.6$  nm (red circles) and  $L_w = 3.43$  nm (black squares), respectively. The open symbols denote the results in the absence of well width fluctuations (No WWFs) while the filled symbols denote the data when well width fluctuations (WWFs) are taken into account.

(black squares). The other well width systems considered here reflect then an intermediate situation. The results in the absence of WWFs (No WWFs) are always indicated by open symbols (square or circle) while the results where WWFs are taken into account are denoted by the filled symbols. We start our analysis here by looking at the QW system with  $L_w = 3.43$  nm (black squares). When comparing the exciton binding energies obtained in the presence and absence of WWFs, we find that the WWF is of secondary importance for this quantity. This finding is consistent with the results of the average exciton binding energy depicted in the inset of Fig. 4. This indicates already that for wider QWs, the wave function overlap is not significantly affected by the presence of WWFs. Again, we will come back to this question below when we discuss the interplay of WWFs and Coulomb effects on the wave functions/charge densities. For the system with  $L_w = 1.6$  nm, the results are given by the (red) circles in Fig. 5. In contrast to the system with  $L_w = 3.43$  nm, we observe that the presence of WWFs can make a noticeable difference to the exciton binding energy in the different configurations. However, there is not a universal trend in the sense that WWFs always lead to an decrease in the exciton binding energy. We have also situations where the WWF leads to an increase in the exciton binding energy (e.g. Configs. 18 and 19). Overall, this reveals that for smaller  $L_w$  values, the presence or absence of WWFs in combination with Coulomb effects significantly affect the electron-hole overlap. For larger well width, this seems not to be the case since the exciton binding energies are almost unaffected by the presence of WWFs compared to the situation where WWFs are absent (cf. Fig. 5).

To shed more light onto wave function localization features and to support explanations given earlier in terms of wave function overlaps, we now turn to examine the

single-particle and many-body (excitonic) charge densities of the considered QWs. Figures 6 and 9 display iso-surface plots of the electron and hole GS charge densities in the presence and absence of WWFs for the QWs with  $L_w = 3.43$  nm and  $L_w = 1.6$  nm, respectively. Here, the results are displayed both for the single-particle states (Single-Particle) as well as when Coulomb interaction effects (Many-Body) are taken into account. The excitonic charge densities have been deduced from reduced density matrices.<sup>8,58</sup> For both systems, the results are shown for a side view (perpendicular to  $c$ -axis) and for a top view (parallel to the  $c$ -axis). The isosurfaces of the charge densities are displayed at 10% (light surface) and 50% (dark surface) of the respective maximum probability densities. Electron charge densities are given in red, hole charge densities in blue. To understand general features, we have selected configurations (Configs.) 4, 11 and 18. These configurations have been selected on the basis of the system with  $L_w = 1.6$  nm since they reflect situations where the WWF leads to a reduction (Config. 4) and an increase (Config. 18) of the exciton binding energy (cf. Fig. 5). The last configuration, Config. 11, represents the situation where the exciton binding is almost unaffected by the presence of WWFs (cf. Fig. 5).

We start our analysis with the QW system of width  $L_w = 3.43$  nm. The charge densities of the above discussed configurations are displayed in Fig. 6. In a first step we look at the single-particle results with and without WWFs (left two columns in Fig. 6). Firstly, due to the presence of the electrostatic built-in field, electron and hole wave functions are separated to opposite interfaces of the QW. Consistent with previous calculations,<sup>5,8,11,12</sup> we find here very strong hole localization effects due to random alloy fluctuations. Keeping in mind that for a given microstructure (configuration) the local alloy arrangement at the lower interface is not changed when including the WWF, the hole wave function remains localized in the same spatial position when comparing the results in the presence and absence of the WWF for the same configuration. However, we observe that the localization features of the electron wave functions, for all configurations, are changed due to the presence of the WWF. We find that the electron wave function is always localized at the upper interface by the WWF. This is consistent with previous theoretical studies.<sup>5,8,30</sup> In the absence of the WWF, the electron wave function is more delocalized but still is perturbed by the alloy microstructure. The origin of the anomalous behavior of the hole GS energy of Config. 18, discussed in Sec. IIIB, can readily be inferred from Fig. 6. We find that for this configuration, the hole GS is localized exceptionally high in the QW. Therefore, the hole state will be significantly affected by local changes in the built-in potential and strain field, introduced by the presence of a WWF (cf. discussion in Sec. III A). This extreme situation results in the feature observed in Fig. 2, that Config. 18 exhibits a slight decrease in hole GS energy with the inclusion of the WWF, in contrast to all other

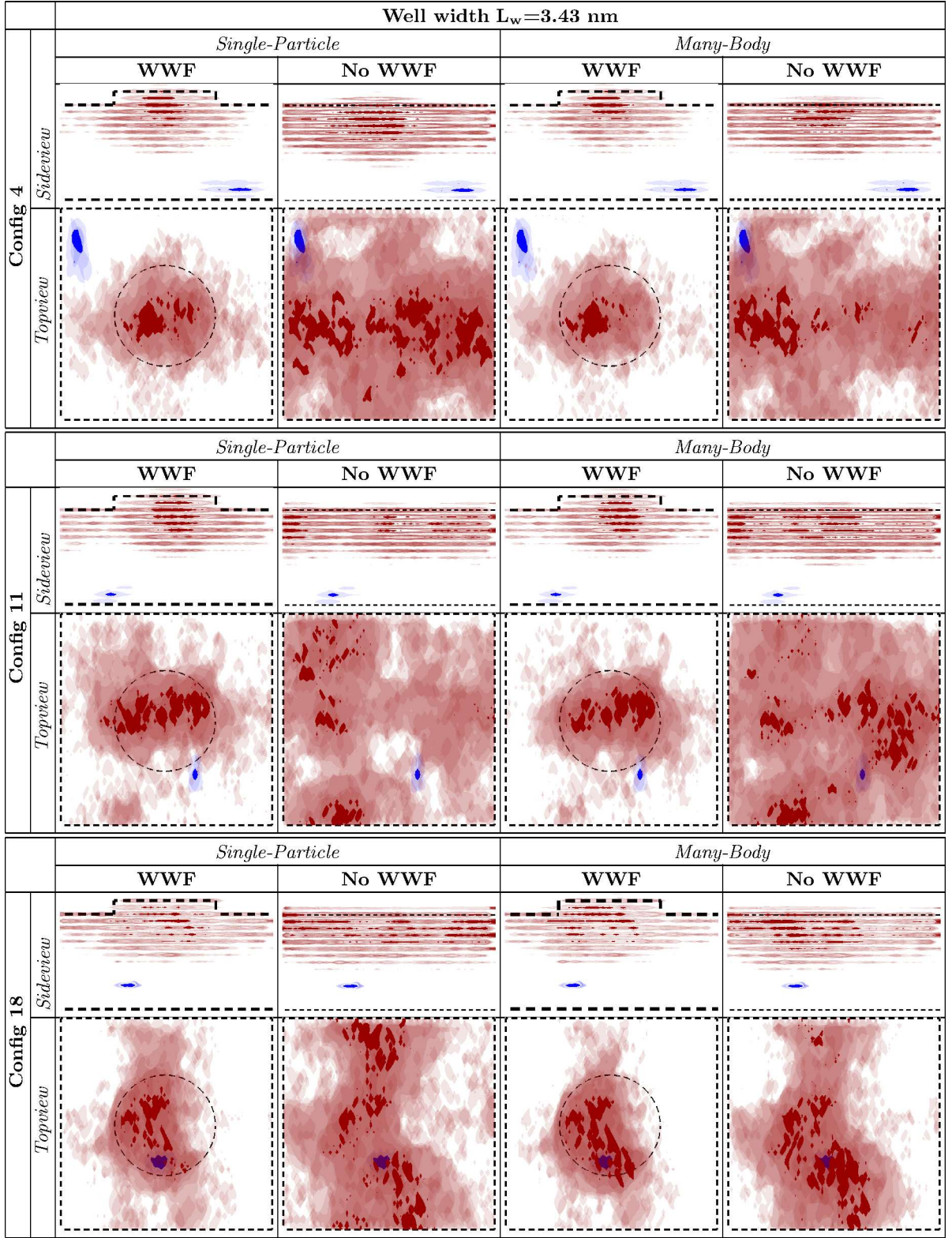


FIG. 6: Isosurface plots of electron (red) and hole (blue) ground state charge densities in the absence (Single-Particle; left) and presence (Many-Body; right) of Coulomb (excitonic) effects for different microscopic configurations and different view points (Sideview: Perpendicular to  $c$ -axis; Topview: Parallel to  $c$ -axis). The light (dark) isosurfaces correspond to 10% (50%) of the maximum charge density. Results are shown with (WWF) and without (No WWF) well width fluctuations. The well width  $L_w$  here is  $L_w = 3.43$  nm.

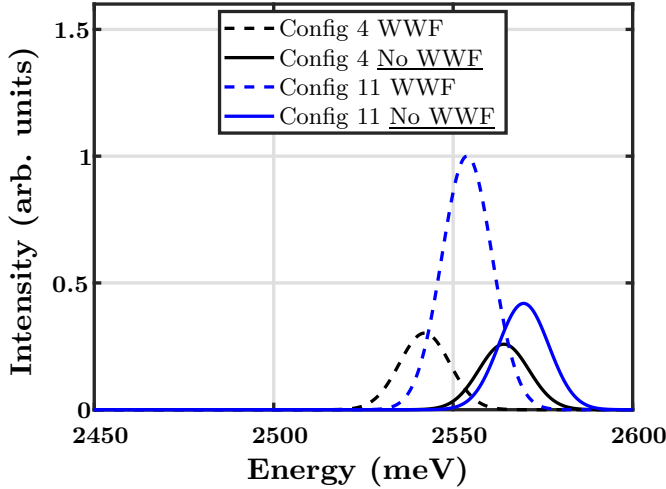


FIG. 7: (Color online) Emission spectrum, neglecting Coulomb effects (single-particle), for Configs. 4 (black) and 11 (blue) in the presence (dashed lines) and absence (solid lines) of well width fluctuations. The well width of the system is  $L_w = 3.43$  nm. The data is normalized to Config. 11 in the presence of well width fluctuations (WWF).

configurations. Furthermore, the spatial separation, both in- and out-of plane, of electron and hole wave functions is unusually small. This leads to an exceptionally large exciton binding energy (cf. Fig. 5).

To further elucidate the connection between carrier localization features and wave function overlap, we have calculated the single-particle emission spectrum for Configs. 4 and 11 in the presence and absence of the WWF. The results are displayed in Fig. 7. We do not present here the results from Config. 18 since the oscillator strength in this case is more than 20 times larger than the largest value of Config. 11. This feature would distract here from the results of the more “standard” configurations. In the following all data are normalized to the results from Config. 11 in the presence of the WWF. For visualization purposes, each peak has been broadened by a Gaussian. As we can see from Fig. 7, the oscillator strength is approximately unchanged in case of Config. 4 when adding or removing the WWF. For Config. 11 the hole wave function is localized near the WWF, explaining why in this case the oscillator strength is higher when the WWF is present compared to the case without the WWF (cf. Fig. 7).

In a second step we study now how the (attractive) Coulomb interaction affects the results. This data is shown on the right hand side of Fig. 6 (Many-Body) with and without the WWF. When comparing these results with the single-particle data, in the presence of the WWF, very little change is observed in the spatial localization features of both electrons and holes. This means that electron and holes are basically “independently” localized. For the case where there is no WWF, we may still say that the electron and hole are independently localized on opposite interfaces of the QW; however, more

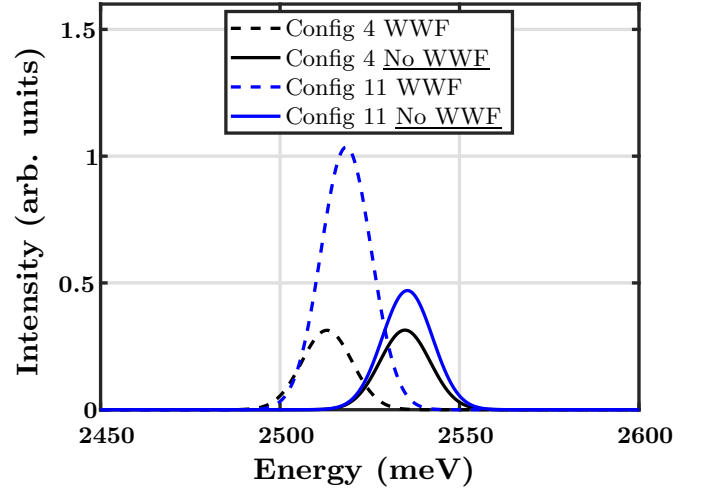


FIG. 8: (Color online) Excitonic emission spectrum for Configs. 4 (black) and 11 (blue) in the presence (dashed lines) and absence (solid lines) of well width fluctuations. The well width of the system is  $L_w = 3.43$  nm. The data is normalized to the spectrum of Config. 11 in the absence of Coulomb effects but in the presence of the well width fluctuation (WWF).

pronounced charge density rearrangements for the electron are observed. This lateral rearrangement of the electron charge density can most easily be seen from the top view. In both cases (Config. 4 and 11), these redistributions of the electron charge density about the hole wave function should lead to a (slight) increase in the GS oscillator strength. The calculated excitonic GS emission spectrum is shown in Fig. 8. Indeed for Config. 11 and Config. 4, the attractive Coulomb interaction leads in both cases, with and without WWFs, to a slight increase in oscillator strength. Note here that the data is again normalized to Config. 11 in the absence of Coulomb effects but in the presence of the WWF (cf. Fig. 7). The finding that with and without WWFs we observe a only slight changes in the oscillator strength is also consistent with the observation that for larger well width the exciton binding energy does not change significantly (cf. Fig. 5) between the two systems (No WWF vs. WWF).

Taking these results together with the observations on the exciton binding energies, Fig. 5, one can draw the following conclusion: For larger QWs, the excitonic binding energy is basically independent of lateral localization features. This can readily be inferred from Configs. 4 and 11 in Fig. 6, where we observe that, despite of the noticeable difference in in-plane separation between the cases with and without WWFs, the differences in the binding energies are negligible. Furthermore, we find here that Config. 18 has the largest binding energy (cf. Fig. 5) of all configurations due to the smallest spatial separation of electron and hole GS wave functions. Also from the comparison of Figs. 7 and 8 we can deduce that the Coulomb effect is of secondary importance for the wave function overlap, at least for large well width. However, the data indicates already that in general reducing



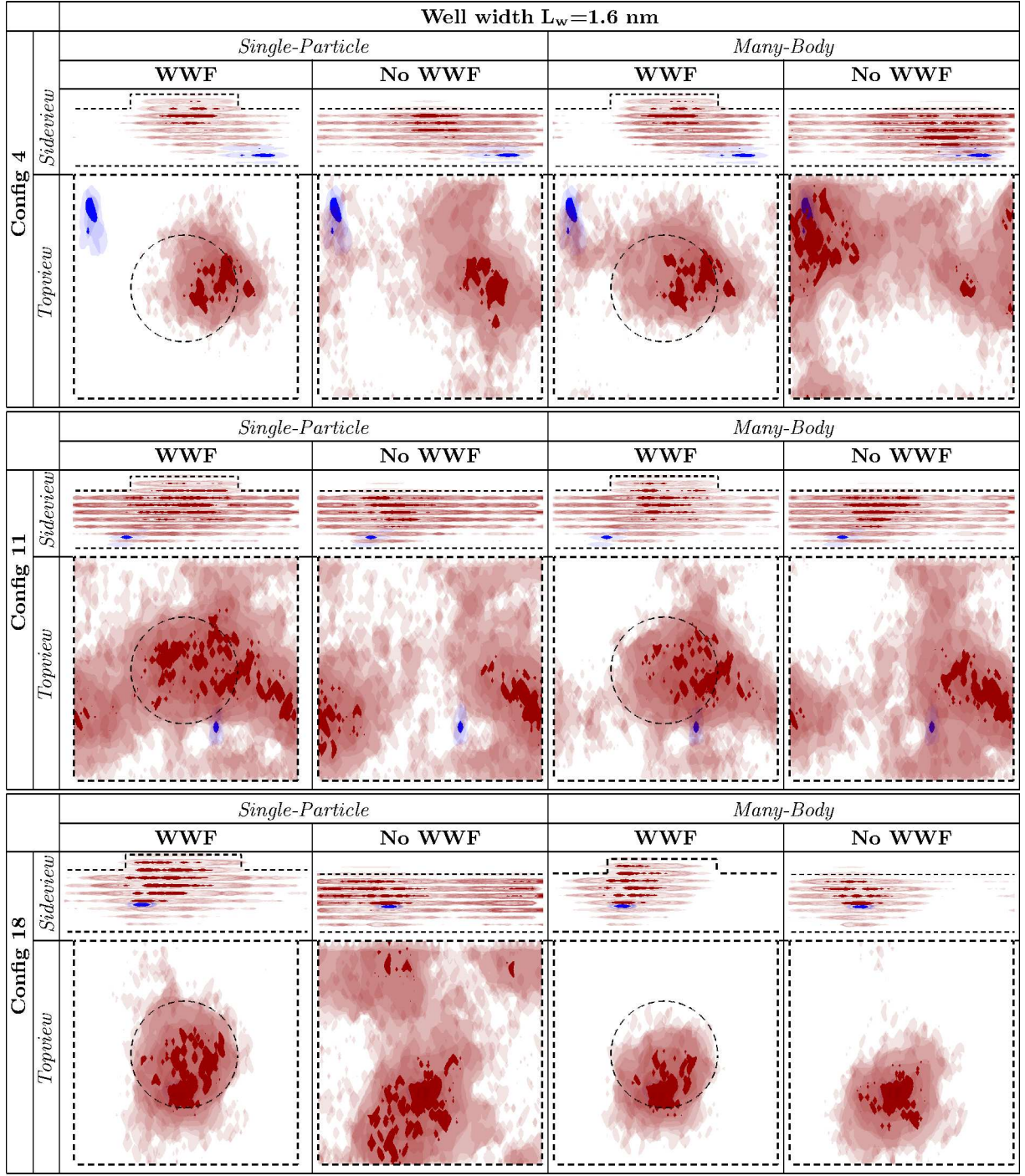


FIG. 9: Isosurface plots of electron (red) and hole (blue) ground state charge densities in the absence (Single-Particle; left) and presence (Many-Body; right) of Coulomb (excitonic) effects for different microscopic configurations and different view points (Sideview: Perpendicular to  $c$ -axis; Topview: Parallel to  $c$ -axis). The light (dark) isosurfaces correspond to 10% (50%) of the maximum charge density. Results are shown with (WWF) and without (No WWF) well width fluctuations. The well width  $L_w$  here is  $L_w = 1.6$  nm.

the QW barrier interface roughness and therefore WWFs should, even for these larger QW width, allow for a redistribution of the (electron) charge density due to Coulomb effects. This gives already indication that Coulomb ef-

fects can reduce the spatial in-plane separation of the carriers. Overall, the oscillator strength should at least slightly benefit from this feature.

Having discussed the  $L_w = 3.43$  nm case, we now turn



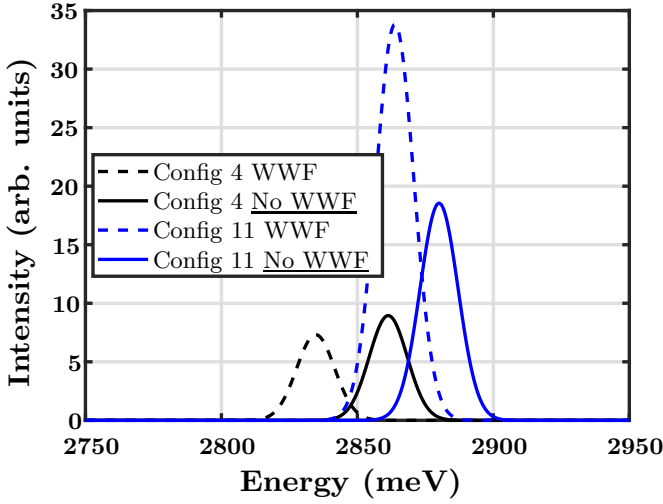


FIG. 10: (Color online) Emission spectrum, neglecting Coulomb effects (single-particle), for Configs. 4 (black) and 11 (blue) in the presence (dashed lines) and absence (solid lines) of well width fluctuations. The well width of the system is  $L_w = 1.6$  nm. The data is normalized to the spectrum of Config. 11 in the absence of Coulomb effects but in the presence of the well width fluctuation (WWF) (cf. Fig. 7).

to the QW system with  $L_w = 1.6$  nm. From Figs. 4 and 5 we know already that, compared to the system with  $L_w = 3.43$  nm, the exciton binding energy is increased in the  $L_w = 1.6$  nm structures on average. Also in Fig. 5 we observe that both WWFs and the microscopic alloy structure lead to a significant variation in the exciton binding energy. To understand these differences, we look first at the electron and hole GS charge densities. These are presented in Fig. 9, using the same configurations as in Fig. 6.

We begin our analysis, as before, by looking at the single-particle properties (first two columns). Note that for each configuration, the hole charge densities are essentially the same as in the  $L_w = 3.43$  nm case, originating from the fact that for a given configuration the alloy microstructure at the lower interface of the well is unchanged when increasing the well width (cf. Sec. II B). The GS electron charge densities, being subject to a different atomic environment, show noticeable differences from the QW with  $L_w = 3.43$  nm. However, the general behavior is similar, with the electron being strongly affected by the combined effect of built-in field and WWFs. Due to the smaller QW width, electron and hole wave functions are less vertically separated, leading to a higher spatial overlap between the wave functions. This is also reflected in the calculated single-particle GS emission spectrum shown in Fig. 10, again for Configs. 4 and 11 with and without WWFs. As before, this data is normalized to the spectrum of Config. 11 for the well with  $L_w = 3.43$  nm in the absence of Coulomb effects but in the presence of the WWF (cf. Fig. 7). Comparing the results for a well width of  $L_w = 1.6$  nm (Fig. 10) with

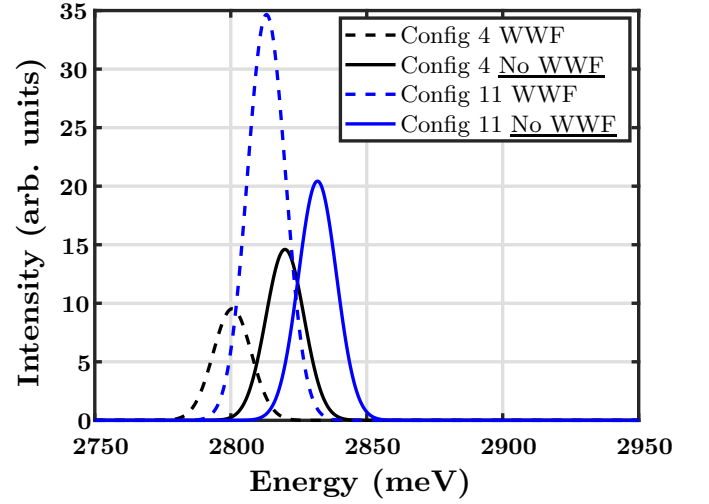


FIG. 11: (Color online) Excitonic emission spectrum for Configs. 4 (black) and 11 (blue) in the presence (dashed lines) and absence (solid lines) of well width fluctuations. The well width of the system is  $L_w = 1.6$  nm. The data is normalized to the spectrum of Config. 11 in the absence of Coulomb effects but in the presence of the well width fluctuation (WWF).

data for  $L_w = 3.43$  nm (Fig. 7), the oscillator strength increases by a factor of order of at least 20. Otherwise, the general features between the two systems are very similar. However, due to the increased spatial electron and hole wave function overlap and consistent with previous discussion, the exciton binding energy is significantly increased for the well with  $L_w = 1.6$  nm when compared to the  $L_w = 3.43$  nm system (cf. Fig. 5).

For the well with  $L_w = 1.6$  nm, a pertinent question now relates to the balance between the enhanced Coulomb effect and the localization “strength” of WWF and random alloy: Is the Coulomb interaction strong enough at this width to overcome the localizing potential of the WWF and mitigate the lateral separation between the electron and hole? To investigate this, we consider the charge densities obtained in the presence of Coulomb effects. These results are shown in the last two columns of Fig. 9 (Many-Body). Initially, we focus our attention on the situation with WWFs. Looking at Config. 4, and comparing with the data from  $L_w = 3.43$  nm (Fig. 6), we observe clearly a stronger redistribution of the electron charge density towards the hole. Similar findings hold for Configs. 11 and 18. However, the carrier localization effects are still largely determined by random alloy contributions and WWFs. In the presence of WWFs, even for the lowest well width studied here and independent of the microscopic configuration, the single-particle picture still gives a very good approximation of the system in terms of its localization features. Thus this system is still consistent with the picture of “independently” localized carriers, as introduced by Morel *et al.*<sup>2</sup> But, when looking at the corresponding excitonic emission spectrum, Fig. 11, and comparing to the single-particle emission spectrum,

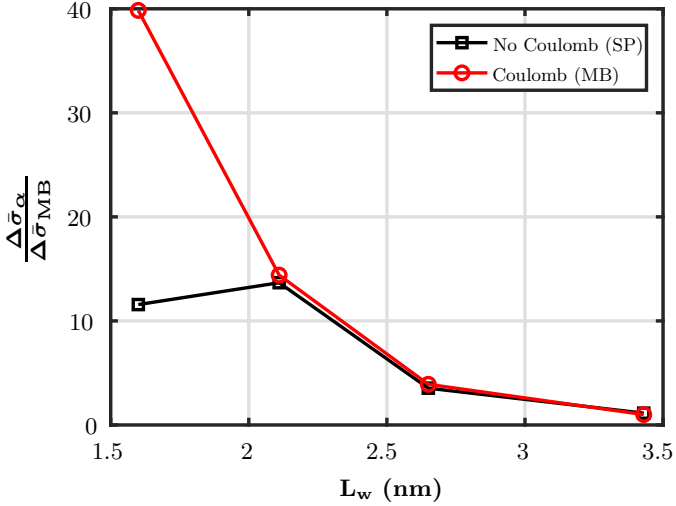


FIG. 12: (Color online) Normalized difference in the average peak oscillator strength,  $\Delta\bar{\sigma}_\alpha(L_w)$ , between the system without and with the WWFs as function of the well width  $L_w$ . The results are shown in presence (red circle) and absence (black squares) of Coulomb effects. More details are given in the text.

Fig. 10, even in the presence of WWFs (dashed lines) the oscillator strength is noticeably affected by the attractive Coulomb effect. Note again, the data is normalized to the spectrum of Config. 11 from Fig. 7. We will come back to the impact of the interplay of Coulomb effects and WWFs on the wave function overlap in more detail below.

Taking the results from the  $L_w = 3.53$  nm and  $L_w = 1.6$  nm cases together we are left with the following picture. Our calculations indicate that the importance of the Coulomb interaction depends strongly on the the vertical separation of the electron and hole wave functions. Thus, in our case here on the the QW width. However, a similar effect would be observed with increasing In content, given that the strain dependent piezoelectric potential increases with increasing In content and thus leads to a stronger out of plane separation of the carrier wave functions.<sup>59</sup> This statement is supported by our recent studies, where we have shown that with increasing In content carrier localization effects of electrons and holes at the QW barrier interface are further enhanced and the out-of plane carrier separation is increased.<sup>10</sup> Furthermore, we find here that WWFs serve as a barrier to the lateral charge density redistribution facilitated by Coulomb effects.

However the situation is less clear cut when WWFs are absent. For the largest well width considered here,  $L_w = 3.43$  nm, charge density redistributions are observed but for instance the oscillator strength or the excitonic binding energies are only slightly affected. But, when reducing the well width these charge redistributions due to Coulomb effects are more pronounced and can partially compensate the in-plane carrier separation.

This argument is supported by the data displayed in Fig. 12, which shows the (normalized) difference in the average peak oscillator strength,  $\frac{\Delta\bar{\sigma}_\alpha(L_w)}{\Delta\bar{\sigma}_{MB}(L_w=3.43\text{ nm})} = \frac{(\bar{\sigma}_\alpha^{\text{NoWWF}}(L_w) - \bar{\sigma}_\alpha^{\text{WWF}}(L_w))}{(\bar{\sigma}_{MB}^{\text{NoWWF}}(L_w=3.43\text{ nm}) - \bar{\sigma}_{MB}^{\text{WWF}}(L_w=3.43\text{ nm}))}$ , between the system without (No WWF) and with WWFs. The results are displayed as a function of the well width  $L_w$ . The index  $\alpha$  denotes if the calculations have been performed in the presence (MB, red circles) or absence (SP, black squares) of Coulomb effects. Here, the data is normalized to  $\Delta\bar{\sigma}_{MB}(L_w = 3.43\text{ nm})$ . Figure 12 reveals that for the largest well width removing the WWF has very little effect on the oscillator strength ( $\Delta\bar{\sigma}_\alpha(L_w = 3.43\text{ nm})/\Delta\bar{\sigma}_{MB}(L_w = 3.43\text{ nm}) \approx 1$ ). However, with decreasing well width  $L_w$ ,  $\Delta\bar{\sigma}_\alpha/\Delta\bar{\sigma}_{MB} \gg 1$ , indicating that the oscillator strength in the absence of the WWF increases on average much more quickly when compared to the situation where the WWF is present. This finding holds also for situation with and without Coulomb effects. Note, the kink in the data without Coulomb effects (black squares) is caused by the extreme configuration 18. When neglecting Config. 18 (not shown)  $\Delta\bar{\sigma}_{SP}(L_w = 1.6\text{ nm})/\Delta\bar{\sigma}_{MB}(L_w = 3.43\text{ nm}) \approx 16$  and  $\Delta\bar{\sigma}_{SP}(L_w = 2.11\text{ nm})/\Delta\bar{\sigma}_{MB}(L_w = 3.43\text{ nm})$  decrease slightly. Overall our analysis strengthens the argument that reducing the roughness of the QW barrier interface can have a significant impact on the optical properties of InGaN/GaN QWs and thus on devices utilizing these. We discuss these benefits in more detail in the following section.

#### D. Comparison with experiment and consequences for radiative recombination in InGaN/GaN QWs

Taking the results of all the above studies into account we can draw here the following conclusions, which are relevant for the radiative recombination dynamics and optical properties of InGaN/GaN QWs. Looking at Fig. 12 we note here that in the extreme case of low well width and no WWFs, Coulomb effects have a very strong impact on  $\Delta\bar{\sigma}_{MB}(L_w)/\Delta\bar{\sigma}_{MB}(L_w = 3.43\text{ nm})$  reflecting the above discussed observation that in the absence of WWFs the spatial in-plane separation can be reduced by the Coulomb effect. This has finding has now two immediate consequences.

First, if the green gap problem is related to in-plane carrier localization effects, as argued in Refs. 11 and 13, reducing the surface roughness of GaN on InGaN might lead to a significant improvement in the device performance, at least for the radiative recombination, given the charge density redistribution due to Coulomb effects and the connected reduction of the spatial in-plane separation. Our finding here is inline with the recent experimental studies focussing on this aspect.<sup>55,60,61</sup> Our calculations confirm and support the recent experimental arguments that understanding and tailoring the QW barrier interface in terms of roughness plays an impor-

tant role for the electronic and optical properties of these systems. Furthermore, our argument that the interface roughness plays a key role for optical properties of these systems might also be related to the experimentally reported enhancement of the PL intensity of InGaN/GaN QWs after reduction of the surface roughness via Hydrogen treatment during growth.<sup>62</sup>

In addition to these device related aspects, our above presented results indicate also potential changes in the fundamental physical properties of the radiative recombination dynamics of InGaN/GaN QWs with varying well width. Here, we find for instance that for some configurations the recombination process may be considered as being driven by exciton localization effects (cf. Configs 4 and 18 in Fig. 9), with the electron localizing about the hole, instead of a picture of independently localized carriers. Reducing the well width and/or the In content further and thus the built-in field, might lead to the situation of exciton localization in general, independent of the microscopic configuration. Therefore, our results give indications that a continuous transition from a system that can be described by independently localized carriers to the case where radiative recombination is determined by exciton localization effects may be achieved. Experimentally such a transition could be observed by changes in the time dependent PL decay curves. For instance a non-single-exponential decay in *c*-plane InGaN/GaN QWs has been often explained by the picture of independently localized carrier.<sup>2,9</sup> For non-polar systems, single-exponential decay curves have been observed and exciton localization effects have been used to explain this behavior.<sup>9,63,64</sup> Interestingly, such an effect of a change in PL decay characteristics has been observed experimentally by Davidson *et al.*<sup>31</sup> and Langer *et al.*<sup>65</sup> in *c*-plane systems. In the experiments of Davidson *et al.*<sup>31</sup> the well width of *c*-plane InGaN/GaN QWs with 13% In has been reduced from 5 nm to 1.25 nm revealing the transition from non-exponential to single-exponential decay curves. In the study of Langer *et al.*<sup>65</sup>, a marked difference in the carrier dynamics of a 2.7 nm and 1.1 nm QW are observed, with the constancy of the PL decay lifetime of the smaller well with carrier density imputed to strong excitonic effects.

Furthermore, Langer *et al.*<sup>65</sup> as well as Hangleiter *et al.*<sup>66</sup> discussed in their work excitonic recombination at room temperature. To achieve such a behavior large exciton binding energies, exceeding the room temperature thermal energy of 26 meV are required. Exciton binding energies of 15-50 meV have been reported in combined theoretical and experimental literature studies on GaN and InGaN QWs.<sup>67,68</sup> These values are in good agreement with our obtained values of 30-50 meV (cf. Fig. 5) for In<sub>0.15</sub>Ga<sub>0.85</sub>N/GaN QWs. Therefore, the here calculated exciton binding energies, which exceed the thermal energy at room temperature, might facilitate the existence of stable excitons at room temperature as reported experimentally.

## IV. CONCLUSION

In summary, we have presented a detailed theoretical analysis of the impact of the interplay between well width, structural inhomogeneities, alloy fluctuations, and Coulomb effects on the electronic and optical properties of InGaN/GaN QWs. This analysis not only gave insight into fundamental properties of this material system, it also revealed possible routes towards the optimization of the radiative recombination process in InGaN-based devices via tailoring their structural properties.

Overall our calculations reveal that for the here studied QW widths  $L_w$ , ranging from  $L_w = 1.6$  nm up to  $L_w = 3.43$  nm, carrier localization effects due to built-in field, well width fluctuations (electrons) and random alloy fluctuations (holes) dominate over the attractive Coulomb interaction between the carriers. At least in terms of wave function localization features, we are left with the picture of “independently” localized carriers, consistent with the concept introduced by Morel *et al.*<sup>2</sup> to explain time-resolved PL spectra *c*-plane InGaN/GaN QWs.

Our data also shows that if well width fluctuations are present, in addition to the built-in field induced out-of-plane wave function separation, an additional in-plane component is present. This component is only slightly affected when Coulomb effects are taken into account. Auf der Maur *et al.*<sup>11</sup> argued that this in-plane separation feature is a key component to the “green gap”, though their calculations neglected well width fluctuations and Coulomb effects.

However, our study shows that in the absence of structural inhomogeneities such as well width fluctuations the situation is less clear cut. In this case, and neglecting Coulomb effects initially, carrier localization effects are introduced by the interplay of random alloy fluctuations and built-in field. Here, we find that hole wave functions are strongly localized by the random alloy fluctuations while the electron wave functions are more delocalized when compared to the situation with a well width fluctuation. But, the electron wave function, in terms of localization features, is perturbed by the random alloy fluctuations. Thus, this gives rise to an in-plane spatial separation of electron and hole wave functions. When including Coulomb effects in the calculations, for larger well width, only slight modifications of the charge densities are observed. However, these results indicated a charge density redistribution of the electron wave function, while the hole charge density is basically unchanged. This feature is more pronounced with decreasing well width, clearly revealing that in the absence of well width fluctuations, the in-plane spatial separation of electron and hole wave functions in a single-particle picture can be reduced by the attractive Coulomb interaction between the carriers.

Therefore, our analysis gives the important finding that reducing the GaN InGaN interface roughness in InGaN/GaN QWs should be extremely beneficial for the radiative recombination in light emitters utilizing this

material system. This originates from the observation that in the absence of well width fluctuations the in-plane spatial carrier localization can be partially compensated by the attractive Coulomb interaction.

While these features are of interest from a device application point of view, especially for the green gap problem, our results also indicate that it might be possible to “tune the physics” of this system by changing the well width. For instance, we observe here that for the smallest well width ( $L_w = 1.6$  nm), for some configurations the electron localizes about the hole due to the attractive Coulomb interaction. Thus we observe here exciton localization features in *c*-plane structures instead of the picture of “independently” localized carriers usually used

to describe the optical properties of these system. Experimentally such a transition could be observed in time resolved PL measurements for instance and has indeed been observed in *c*-plane systems.<sup>31,65</sup> Moreover, our here presented analysis, in terms of carrier localization and impact of Coulomb effects should also be of interest for studies on novel monolayer InGaN/GaN systems.<sup>69</sup>

## Acknowledgments

This work was supported by Science Foundation Ireland (project number 13/SIRG/2210).

- <sup>1</sup> Y.-H. Cho, G. H. Gainer, A. J. Fischer, J. J. Song, S. Keller, U. K. Mishra, and S. P. DenBaars, *Appl. Phys. Lett.* **73**, 1370 (1998).
- <sup>2</sup> A. Morel, P. Lefebvre, S. Kalliakos, T. Taliercio, T. Bretagnon, and B. Gil, *Physical Review B* **68**, 045331 (2003).
- <sup>3</sup> D. M. Graham, A. Soltani-Vala, P. Dawson, M. J. Godfrey, T. M. Smeeton, J. S. Barnard, M. J. Kappers, C. J. Humphreys, and E. J. Thrush, *Journal of Applied Physics* **97**, 103508 (2002).
- <sup>4</sup> S. F. Chichibu, A. Uedono, T. Onuma, B. A. Haskell, A. Chakraborty, T. Koyama, P. T. Fini, S. Keller, S. P. Denbaars, J. S. Speck, et al., *Nature Materials* **5**, 810 (2006).
- <sup>5</sup> D. Watson-Parris, M. J. Godfrey, P. Dawson, R. A. Oliver, M. J. Galtrey, M. J. Kappers, and C. J. Humphreys, *Phys. Rev. B* **83**, 115321 (2011).
- <sup>6</sup> S. Hammersley, D. Watson-Parris, P. Dawson, M. J. Godfrey, T. J. Badcock, M. J. Kappers, C. McAleese, R. A. Oliver, and C. J. Humphreys, *Journal of Applied Physics* **111**, 083512 (2012).
- <sup>7</sup> T.-J. Yang, R. Shivaraman, J. S. Speck, and Y.-R. Wu, *Journal of Applied Physics* **116**, 113104 (2014).
- <sup>8</sup> S. Schulz, M. A. Caro, C. Coughlan, and E. P. O'Reilly, *Physical Review B* **91**, 035439 (2015).
- <sup>9</sup> P. Dawson, S. Schulz, R. A. Oliver, M. J. Kappers, and C. J. Humphreys, *Journal of Applied Physics* **119**, 181505 (2016).
- <sup>10</sup> D. P. Tanner, M. A. Caro, E. P. O'Reilly, and S. Schulz, *RSC Adv.* **6**, 64513 (2016).
- <sup>11</sup> M. Auf der Maur, A. Pecchia, G. Penazzi, W. Rodrigues, and A. Di Carlo, *Physical Review Letters* **116**, 027401 (2016).
- <sup>12</sup> C. M. Jones, C.-H. Teng, Q. Yan, P.-C. Ku, and E. Kioupakis, *Appl. Phys. Lett.* **111**, 113501 (2017).
- <sup>13</sup> S. Y. Karpov, *Photon. Res.* **5**, A7 (2017).
- <sup>14</sup> M. Filoche, M. Piccardo, Y.-R. Wu, C.-K. Li, C. Weisbuch, and S. Mayboroda, *Phys. Rev. B* **95**, 144204 (2017).
- <sup>15</sup> C.-K. Li, M. Piccardo, L.-S. Lu, S. Mayboroda, L. Martinelli, J. Peretti, J. S. Speck, C. Weisbuch, M. Filoche, and Y.-R. Wu, *Phys. Rev. B* **95**, 144206 (2017).
- <sup>16</sup> M. Piccardo, C.-K. Li, Y.-R. Wu, J. S. Speck, B. Bonef, R. M. Farrell, M. Filoche, L. Martinelli, J. Peretti, and C. Weisbuch, *Phys. Rev. B* **95**, 144205 (2017).
- <sup>17</sup> M. A. Sousa, T. C. Esteves, N. B. Sedrine, J. Rodrigues, M. B. Lourenco, A. Redondo-Cubero, E. Alves, K. P. O'Donnell, M. Bockowski, C. Wetzel, et al., *Sci. Report* **5**, 9703 (2015).
- <sup>18</sup> W. E. Blenkhorn, S. Schulz, D. S. P. Tanner, R. A. Oliver, M. J. Kappers, C. J. Humphreys, and P. Dawson, *J. Phys.: Condens. Matter* **30**, 175303 (2018).
- <sup>19</sup> S. Chichibu, K. Wada, and S. Nakamura, *Applied Physics Letters* **71**, 2346 (1997).
- <sup>20</sup> I. Ho and G. B. Stringfellow, *Applied Physics Letters* **69**, 2701 (1996).
- <sup>21</sup> T. M. Smeeton, M. J. Kappers, J. S. Barnard, M. E. Vickers, and C. J. Humphreys, *Applied Physics Letters* **83**, 5419 (2003).
- <sup>22</sup> M. J. Galtrey, R. A. Oliver, M. J. Kappers, C. J. Humphreys, D. J. Stokes, P. H. Clifton, and A. Cerezo, *Applied Physics Letters* **90**, 061903 (2007).
- <sup>23</sup> S. Y. Karpov, *MRS Internet Journal of Nitride Semiconductor Research* **3**, e16 (1998).
- <sup>24</sup> G. Sarau, M. Heilmann, M. Latzel, and S. Christiansen, *Nanoscale* **6**, 11953 (2014).
- <sup>25</sup> C.-K. Tan, W. Sun, J. J. Wierer, and N. Tansu, *AIP Advances* **7**, 035212 (2017).
- <sup>26</sup> E. Kioupakis, P. Rinke, K. T. Delaney, and C. G. V. de Walle, *Applied Physics Letters* **98**, 161107 (2011).
- <sup>27</sup> M. Binder, A. Nirschl, R. Zeisel, T. Hager, H.-J. Lugauer, M. Sabathil, D. Bougeard, J. Wagner, and B. Galler, *Applied Physics Letters* **103**, 071108 (2013).
- <sup>28</sup> J. Iveland, L. Martinelli, J. Peretti, J. S. Speck, and C. Weisbuch, *Phys. Rev. Lett.* **110**, 177406 (2013).
- <sup>29</sup> B. Galler, H.-J. Lugauer, M. Binder, R. Hollweck, Y. Folwill, A. Nirschl, A. Gomez-Iglesias, B. Hahn, J. Wagner, and M. Sabathil, *Applied Physics Express* **6**, 112101 (2013).
- <sup>30</sup> D. T. S. Watson-Parris, *Carrier Localization in InGaN/GaN Quantum Wells*, PhD Thesis (University of Manchester, <https://www.escholar.manchester.ac.uk/uk-ac-man-scw:132844>, 2011).
- <sup>31</sup> J. A. Davidson, P. Dawson, T. Wang, T. Sugahara, J. W. Orton, and S. Sakai, *Semiconductor Science and Technology* **15**, 497 (2000).
- <sup>32</sup> B. Monemar, J. P. Bergman, J. Dalfors, G. Pozina, B. Serenelius, P. Holtz, H. Amano, and I. Akasaki, *MRS Internet Journal of Nitride Semiconductor Research* **4**, e16 (1999).
- <sup>33</sup> Y. Narukawa, Y. Kawakami, S. Fujita, S. Fujita, and



- S. Nakamura, Phys. Rev. B **55**, R1938 (1997).
- <sup>34</sup> S. J. Plimpton, Journal of Computational Physics **117**, 1 (1995).
  - <sup>35</sup> R. M. Martin, Physical Review B **1**, 4005 (1970).
  - <sup>36</sup> M. A. Caro, S. Schulz, and E. P. O'Reilly, Physical Review B **88**, 214103 (2013).
  - <sup>37</sup> T. Saito and Y. Arakawa, Physica E (Amsterdam) **15**, 169 (2002).
  - <sup>38</sup> M. Zielinski, W. Jaskolski, J. Aizpurua, and G. W. Bryant, Acta Physica Polonica A **108**, 929 (2005).
  - <sup>39</sup> K. Schuh, S. Barthel, O. Marquardt, T. Hickel, J. Neugebauer, G. Czycholl, and F. Jahnke, Appl. Phys. Lett. **100**, 092103 (2012).
  - <sup>40</sup> N. Baer, S. Schulz, P. Gartner, S. Schumacher, G. Czycholl, and F. Jahnke, Phys. Rev. B **76**, 075310 (2007).
  - <sup>41</sup> Z. H. Levine and S. G. Louie, Phys. Rev. B **25**, 6310 (1982).
  - <sup>42</sup> A. Franceschetti, H. Fu, L. W. Wang, and A. Zunger, Phys. Rev. B **60**, 1819 (1999).
  - <sup>43</sup> S. Nakamura and S. F. Chichibu, eds., *Introduction to Nitride Semiconductor Blue Lasers and Light Emitting Diodes* (CRC Press, 2000).
  - <sup>44</sup> V. Y. Davydov, A. A. Klochikhin, M. B. Smirnov, V. V. Emtsev, V. D. Petrikov, I. A. Abroyan, A. I. Titov, I. N. Goncharuk, A. N. Smirnov, V. V. Mamutin, et al., Physica Status Solidi B **216**, 779 (1999).
  - <sup>45</sup> M. Swiderski and M. Zielinski, Phys. Rev. B **95**, 125407 (2017).
  - <sup>46</sup> W. Sheng, S.-J. Cheng, , and P. Hawrylak, Phys. Rev. B **71**, 035316 (2005).
  - <sup>47</sup> E. Goldmann, S. Barthel, M. Florian, K. Schuh, and F. Jahnke, Appl. Phys. Lett. **103**, 242102 (2013).
  - <sup>48</sup> S. Schulz, S. Schumacher, and G. Czycholl, Phys. Rev. B **73**, 245327 (2006).
  - <sup>49</sup> M. J. Galtrey, R. A. Oliver, M. J. Kappers, and C. J. Humphreys, Applied Physics Letters **90**, 061903 (2007).
  - <sup>50</sup> P. M. McBride, Q. Yan, and C. G. Van de Walle, Appl. Phys. Lett. **105**, 083507 (2014).
  - <sup>51</sup> B. Monemar, J. P. Bergman, J. Dalfors, G. Pozina, B. E. Sernelius, P. O. Holtz, H. Amano, and I. Akasaki, MRS Internet Journal of Nitride Semiconductor Research **4**, e16 (1999).
  - <sup>52</sup> L. Hoffmann, H. Bremers, H. Jönen, U. Rossow, M. Schowalter, T. Mehrtens, A. Rosenauer, and A. Hangleiter, Applied Physics Letters **102**, 102110 (2013).
  - <sup>53</sup> R. A. Oliver, S. E. Bennett, T. Zhu, D. J. Beesley, M. J. Kappers, D. W. Saxey, A. Cerezo, and C. J. Humphreys, J. Phys. D: Appl. Phys. **43**, 354003 (2010).
  - <sup>54</sup> T. Sato, K. Nakano, H. Matsumoto, S. Torikawa, I. Nakatani, M. Kiyohara, and T. Isshiki, IOP Conf. Series: Journal of Physics: Conf. Series **902**, 012019 (2017).
  - <sup>55</sup> F. Massabuau, N. Piot, M. Frentrup, X. Wang, Q. Avenas, M. Kappers, C. Humphreys, and R. Oliver, Phys. Status Solidi B **254**, 1600664 (2017).
  - <sup>56</sup> S. F. Chichibu, A. C. Abare, M. S. Minsky, S. Keller, S. B. Fleischer, J. E. Bowers, E. Hu, U. K. Mishra, L. A. Coldren, S. P. DenBaars, et al., Applied Physics Letters **73**, 2006 (1998).
  - <sup>57</sup> K. P. O'Donnell, R. W. Martin, and P. G. Middleton, Physical Review Letters **82**, 237 (1999).
  - <sup>58</sup> S. Barthel, K. Schuh, O. Marquardt, T. Hickel, J. Neugebauer, F. Jahnke, and G. Czycholl, Eur. Phys. J. B **86**, 449 (2013).
  - <sup>59</sup> D. P. Williams, S. Schulz, A. D. Andreev, and E. P. O'Reilly, J. Sel. Top. Quant. Electron. **15**, 1092 (2009).
  - <sup>60</sup> Y.-C. Cheng, C.-M. Wu, M.-K. Chen, C. C. Yang, and Z.-C. Feng, Appl. Phys. Lett. **84**, 5422 (2004).
  - <sup>61</sup> Z. Wu, X. Shen, H. Xiong, Q. Li, J. Kang, Z. Fang, F. Lin, B. Yang, S. Lin, W. Shen, et al., Applied Physics A **122**, 108 (2016).
  - <sup>62</sup> Y. Zhu, T. Lu, X. Zhou, G. Zhao, H. Dong, Z. Jia, X. Liu, and B. Xu, Nanoscale Research Letters **12**, 321 (2017), ISSN 1556-276X.
  - <sup>63</sup> S. Marcinkevičius, K. M. Kelchner, L. Y. Kuritzky, S. Nakamura, S. P. DenBaars, and J. S. Speck, Appl. Phys. Lett. **103**, 111107 (2013).
  - <sup>64</sup> S. Schulz, D. P. Tanner, E. P. O'Reilly, M. A. Caro, T. L. Martin, P. A. J. Bagot, M. P. Moody, F. Tang, J. T. Griffiths, F. Oehler, et al., Physical Review B **92**, 235419 (2015).
  - <sup>65</sup> T. Langer, A. Chernikov, D. Kalincev, M. Gerhard, H. Bremers, U. Rossow, M. Koch, and A. Hangleiter, Applied Physics Letters **103**, 202106 (2013).
  - <sup>66</sup> A. Hangleiter, Z. Jin, M. Gerhard, D. Kalincev, T. Langer, H. Bremers, U. Rossow, M. Koch, M. Bonn, and D. Turchinovich, Phys. Rev. B **92**, 241305(R) (2015).
  - <sup>67</sup> P. Bigenwald, P. Lefebvre, T. Bretagnon, and B. Gil, Physica Status Sol. (b) **216**, 371 (1999).
  - <sup>68</sup> S. Lahmann, F. Hitzel, U. Rossow, and A. Hangleiter, Physica Status Sol. (c) **0**, 2202 (2003).
  - <sup>69</sup> D. Ma, X. Rong, X. Zheng, W. Wang, P. Wang, T. Schulz, M. Albrecht, S. Metzner, M. Müller, O. August, et al., Sci. Rep. **7**, 46420 (2017).